Heart and Vessels (2019) 34:1221–1229
https://doi.org/10.1007/s00380-018-01336-3

ORIGINAL ARTICLE

MicroRNA-19b-1 reverses ischaemia-induced heart failure by inhibiting cardiomyocyte apoptosis and targeting Bcl2 l11/BIM

Wenbo Yang[1] · Yanxin Han[1] · Chendie Yang[1] · Yanjia Chen[1] · Weilin Zhao[1] · Xiuxiu Su[1] · Ke Yang[1,2] · Wei Jin[1]

Received: 11 June 2018 / Accepted: 28 December 2018 / Published online: 3 January 2019

Abstract

Ischaemia induces cardiac apoptosis and leads to a loss of cardiac function and heart failure after myocardial infarction. MicroRNA-19b-1 (miR-19b-1), a key member of the miR-17/92 cluster, plays crucial roles in inhibiting apoptosis. However, the role of miR-19b-1 in ischaemia-induced heart failure remains unknown. In this study, ischaemia resulted in cardiac apoptosis and the suppression of miR-19b-1 expression, whereas miR-19b-1 overexpression inhibited ischaemia-induced cardiac apoptosis in vivo and in vitro. Moreover, miR-19b-1 not only attenuated the infarct size but also ameliorated heart failure after myocardial infarction, including the changes in the left ventricular ejection fraction and volume load. Mechanically, miR-19-1 targeted and downregulated the mRNA and protein expression of Bcl2l11/BIM, a pro-apoptotic gene of the Bcl-2 family. Together, these results revealed an essential role of miR-19b-1 in ischaemia-induced heart failure.

Keywords MicroRNA-19b-1 · Heart failure · Myocardial infarction · Cardiac apoptosis · Bcl2-like 11

Introduction

Despite the recent dramatic advancements in cardioprotective therapies, heart failure (HF) is still an incurable and fatal condition that imposes a heavy burden on patients and society [1]. Cardiomyocyte apoptosis in the ischaemic region leads to an irreversible loss of cardiac function due to the weak self-renewal capacity of cardiomyocytes, which limits the benefits of current therapies [2–4]. MicroRNA-19b-1 (miR-19b-1) is a key microRNA (miRNA) in the miR-17/92 cluster [5, 6], and a deficiency in this miRNA causes a ventricular septal defect and a short life span in mice [7]. In cardiovascular diseases, miR-19b-1 was reported to be an antithrombotic protective factor in patients with unstable angina [8] and a potential biomarker of aortic stenosis [9] and human cell ageing [10]. Additionally, miR-19b-1 also plays vital roles in cardiac fibroblast proliferation and migration [11], and attenuates tumour necrosis factor-alpha-induced endothelial cell apoptosis [12]. However, the relationship between miR-19b-1 and HF after myocardial infarction (MI) has not been elucidated.

Notably, miRNAs exert their regulatory functions by targeting multiple genes [13–15]. According to recent studies, miR-19b-1 enhances the resistance of acute T-cell lymphoblastic leukaemia [16] and non-small cell lung cancer cells to apoptosis [17] by targeting the Bcl2-like 11 (Bcl2 l11) gene. The Bcl-2-interacting mediator of cell death (BIM) protein, which is encoded by Bcl2 l11, contains only Bcl-2 homology domain 3 and acts as a proapoptotic activator by interacting with other Bcl-2 family proteins (such as Bcl-2) [18]. However, researchers have not yet determined whether miR-19b-1 attenuates ischaemia-induced cardiomyocyte apoptosis in patients with post-MI HF by inhibiting Bcl2 l11/BIM expression.

In this study, we hypothesised that MI induces cardiomyocyte apoptosis and suppresses miR-19b-1 expression, whereas the overexpression of miR-19b-1 prevents cardiomyocyte apoptosis and improves cardiac function, thus antagonising the ischaemia-induced HF by targeting Bcl2

Wenbo Yang, Yanxin Han and Chendie Yang contributed equally to this work.

✉ Ke Yang
ykk_ykkk@126.com

✉ Wei Jin
jinwei1125@126.com

[1] Department of Cardiology, Ruijin Hospital, Shanghai Jiao Tong University School of Medicine, No 197 Ruijin 2nd Road, Shanghai 200025, People's Republic of China

[2] Institute of Cardiovascular Disease, Shanghai Jiao Tong University School of Medicine, Shanghai, People's Republic of China

l11/BIM. These effects imply that miR-19b-1 represents a promising and effective treatment to prevent ischaemia-induced HF in the future.

Methods

Reagents and antibodies

The lentiviral vector, miR-19b-1-overexpressing lentivirus, and *Renilla*_luciferase plasmid as well as the wild-type and mutant Bcl2 l11-firefly_luciferase plasmids were constructed by GeneChem Corporation (Shanghai, China). Negative control and miR-19b-1 mimics were supplied by RiboBio, Ltd. (Guangzhou, China). Collagenase type 2 was obtained from Worthington Biochemical Corporation (NJ, USA). DMEM/F-12 (Gibco™), 0.25% Trypsin-EDTA (Gibco™), foetal bovine serum (Gibco™), hank's balanced salt solution (Gibco™), penicillin–streptomycin (Gibco™), Lipofectamine 2000 (Invitrogen), Opti-MEM (Invitrogen), TRIzol reagent (Invitrogen) and a TaqMan™ miRNA assay kit were purchased from Thermo Fisher Scientific (MA, USA). The miRNA isolation kit was supplied by TianGen Biotech Corporation (Beijing, China). The AMV reverse transcription system was purchased from Promega (WI, USA). The SYBR® premix DimerEraser™ was purchased from TaKaRa Biotechnology Corporation, Ltd. (Dalian, China). An in situ cell death-detection kit (Roche Applied Science) and an α-tubulin antibody were obtained from Sigma-Aldrich Corporation (Darmstadt, Germany). The BIM antibody, CD31 antibody and HRP-conjugated mouse and rabbit IgGs were obtained from Cell Signalling Technology (MA, USA). The CD68 antibody was purchased from Abcam Plc. (Cambridge, UK).

Animal models

All animal experimental protocols were approved by the Laboratory Animal Ethics Committee of Rui Jin Hospital. The animal model of MI was established by permanently ligating the left anterior descending (LAD) arteries of 8-week-old C57BL/6 mice, as previously described [19, 20]. Briefly, mice were anaesthetized with 1.0–1.5% isoflurane and connected to a mechanical ventilation device, while a left thoracotomy was performed at the fourth intercostal rib space. The LAD artery was ligated with a 7-0 silk suture, and the thoracic incision was closed with a 5-0 silk suture. Lentivirus-infected mice received multi-point intramyocardial injections of 5×10^6 transducing units of the lentivirus vector (Let-blank) or miR-19b-1-overexpressing lentivirus [Let-miR-19b-1(+)] in 10 μL of a phosphate buffer solution during the LAD artery ligation surgery.

Echocardiography

The left ventricular ejection fraction (LVEF) and fractional shortening (FS) were assessed before and once a week after the surgery with a Vevo 2100 instrument (FUJIFILM Visual Sonics, ON, Canada) equipped with an MS-400 imaging transducer. M-mode tracking was performed from the long axis of the heart at the papillary muscle level.

Pressure–volume loop analysis

Invasive pressure–volume loop analysis was performed in mice with MI at the 4th week under general anaesthesia (1.0–1.5% isoflurane). A 1.2-Fr pressure–volume conductance catheter (Transonic Science, Inc., ON, Canada) was introduced into the right carotid artery and pushed forward into the left ventricle. The data were recorded with an iWork system and analysed with LabScribe2 software (NH, USA). After the experiment, the hearts of the anaesthetized mice were harvested for histological analyses.

Histological analysis and infarct size determination

Hearts were fixed with 4% paraformaldehyde, embedded in paraffin, and cut into 5-μm-thick sections. Sections were analysed by performing haematoxylin and eosin (H&E) staining and Masson's trichrome staining to observe the heart tissue morphology. The infarct size was determined by the total infarct circumference divided by the total left ventricle circumference (× 100%). Immunohistochemical staining was performed using the anti-CD31 antibody (1:100) and anti-CD68 antibody (1:100) for 24 h at 4°C and horseradish peroxidase-linked anti-rabbit antibody (1:500) for 60 min at room temperature. Then, the slides were incubated with 3, 3′-diaminobenzidine and counterstained with hematoxylin. Images were captured under a microscope (Olympus Corporation, Tokyo, Japan) and quantified using ImageJ software (National Institutes of Health, MD, USA).

TUNEL staining

The in situ cell death-detection kit was used for TUNEL staining according to the manufacturer's instructions. Cell nuclei were counterstained with DAPI. Images were acquired with an Olympus microscope and analysed with ImageJ software.

Isolation and culture of primary murine cardiomyocytes

Hearts from 3-day-old neonatal C57BL/6 mice were cut into small pieces and digested with an enzyme mixture comprising 0.08% trypsin and 0.05% collagenase type 2 overnight at 4 °C. Tissue lysates were blended with an equal volume of culture medium comprising DMEM/F-12, 15% foetal bovine serum, 1% penicillin–streptomycin and 0.1 mmol/L bromodeoxyuridine. After centrifugation at 1000 rpm for 10 min, cells were resuspended in 10 mL of culture medium and cultured for 60 min. Then, the supernatant was collected into a 65-mm Petri dish, and cardiomyocytes adhered to the dish after 48 h of cultivation.

Hypoxia of cardiomyocytes

Cardiomyocytes were seeded into a 65-mm Petri dish and exposed to a corresponding stimulus, followed by a change of the culture medium to DMEM/F-12 lacking foetal bovine serum. Then, cardiomyocytes were subjected to hypoxic (2% O_2, 5% CO_2, and 93% N_2) or normoxic (5% CO_2 and 21% O_2) conditions for 3 h before harvest.

Culture of endothelial cells and macrophages

Human umbilical vein endothelial cells (HUVECs) were cultured in endothelial cell medium with 5% foetal bovine serum and 1% endothelial cell growth supplement (ScienCell Research Laboratories, Inc., CA, USA) at 37 °C and 5% CO2. The whole blood was collected from the healthy donors, and then the monocytes were isolated with Ficoll-Paque separation (GE Healthcare). The collected monocytes were differentiated with 100 ng/mL M-CSF (PeproTech, London, UK) for 3 days. Non-adherent cells were washed off, and the remaining adherent cells (monocytes derived macrophages) were maintained in RPMI 1640 medium supplemented with 20% foetal bovine serum, 1% penicillin/streptomycin, and 2% L-glutamine. Endothelial cells and macrophages were subjected to hypoxic (2% O_2, 5% CO_2, and 93% N_2) or normoxic (5% CO_2 and 21% O_2) conditions for 3 h before harvest. The culture medium was changed into endothelial cell medium or RPMI 1640 without foetal bovine serum before hypoxia.

Quantitative real-time PCR

Total RNA was extracted from cultured cells using the TRIzol reagent according to the manufacturer's instructions. The AMV reverse transcription system and SYBR® premix DimerEraser™ were used for the first-stand cDNA synthesis and analysis of mRNA expression, respectively. The miRNA isolation kit and TaqMan miRNA assay kit were used to extract miRNAs and detect their relative expression, respectively. Quantitative real-time PCR was performed using a StepOne™ system (Applied Biosystems, CA, USA).

Oligonucleotide transfection

Cardiomyocytes were transfected with 100 nM negative control (NC) or miR-19b-1 mimic using Lipofectamine 2000 and Opti-MEM according to the manufacturer's instructions. Experiments were performed 48 h after the oligonucleotide transfection.

Luciferase reporter assay

The 3′-UTRs of the wild-type and mutant mouse Bcl2 l11 genes containing predicted miR-19b-1 target regions were inserted into the firefly_luciferase plasmid. The *Renilla*_luciferase plasmid was used as a reference. For the luciferase reporter assay, the wild-type (3′-UTR-Bcl2 l11-WT) or mutant Bcl2 l11 (3′-UTR-Bcl2 l11-Mut) reporter plasmid was co-transfected with the NC or miR-19b-1 mimic and the 3′-UTR-*Renilla*_luciferase plasmid into 293T cells using Lipofectamine 2000. Luciferase activity was detected 48 h after transfection using a dual-luciferase assay kit.

Western blotting

Protein lysates were obtained from cultured cardiomyocytes. Equal amounts of protein (20 μg) were separated by sodium dodecyl sulphate polyacrylamide gel electrophoresis and electrotransferred onto polyvinylidene difluoride membranes. Membranes were then incubated with primary antibodies against BIM (1:1000) or α-tubulin (1:2000) overnight at 4 °C, followed by incubation with horseradish peroxidase-conjugated rabbit or mouse IgG (1:2000) for 1 h at room temperature. After the membranes were washed 3 times, immunoreactive bands were detected with an electrochemiluminescence system, and the density of each band was quantified using ImageJ software.

Statistical analysis

Experimental data are presented as the means ± SD. Differences between two groups were evaluated using Student's *t* test. All results were analysed using two-sided tests, and the value of the significance level, α, was defined as 0.05. Statistical analyses were performed with IBM SPSS statistics version 22 (IBM Corporation, NY, USA).

Results

Ischaemia suppressed cardiac miR-19b-1 expression

Because hypoxia is the main factor contributing to cardiac apoptosis in post-MI HF, primary cardiomyocytes were cultured from neonatal C57BL/6 mice and exposed to hypoxia (2% O_2) or normoxia (21% O_2) for 3 h to measure the levels of miR-19b-1 and its related miRNA cluster (miR-17/92 cluster). Compared with the normoxia treatment, hypoxia downregulated all miRNAs of the miR-17/92 cluster (miR-19b-1 = 0.57-fold, $p = 0.003$; miR-92a-1 = 0.67-fold, $p = 0.017$; miR-17 = 0.77-fold, $p = 0.001$; miR-20a = 0.73-fold, $p = 0.003$; miR-18a = 0.82-fold, $p = 0.071$; miR-19a = 0.92-fold, $p = 0.408$; Fig. 1a). Among the miRNAs of the miR-17/92 cluster, miR-19b-1 exhibited the most significant decrease in expression in hypoxic cardiomyocytes.

Based on miR-19b-1 expression in cardiomyocytes cultured under hypoxic conditions in vitro, the levels of miR-19b-1 were measured in the mouse models of MI from days 1 to 28. The expression of miR-19b-1 exhibited a decreasing tendency from days 1 to 14 but increased to approximately that in the sham group on day 28 (Fig. 1b). In addition, the levels of miR-19b-1 in endothelial cells and macrophages 3 h post hypoxia were also measured in vivo. However, there were no differences observed between hypoxia group and normoxia group (Fig. 1c, d).

MiR-19b-1 reduced the infarct size and restored the left ventricular cardiac function

Because miR-19b-1 expression was suppressed in cardiomyocytes under MI conditions, we hypothesised that rescuing the miR-19b-1 level would reduce the cardiac infarct size and restore cardiac function. To test this hypothesis, a lentiviral vector (Let-blank) or miR-19b-1-overexpressing lentivirus [Let-miR-19b-1(+)] was injected into the border zone of the infarcted myocardium to observe its effects on the infarct size and left ventricular systolic function.

The results of H&E and Masson's trichrome staining revealed a much smaller infarct size in the Let-miR-19b-1(+) group than in the Let-blank group [Let-miR-19b-1(+): 40.95% ± 9.56% versus Let-blank: 59.03% ± 12.51%, $p = 0.0218$] at the 4th week after MI surgery (Fig. 2a). Echocardiography revealed substantial improvements in the left ventricular systolic function in the Let-miR-19b-1(+) mice compared to that in the Let-blank mice with MI. Notably, miR-19b-1(+) prevented the decrease in the LVEF [Let-miR-19b-1(+): 49.43% ± 7.23% versus Let-blank: 37.93% ± 13.06%, $p = 0.046$] and FS [Let-miR-19b-1(+): 25.00% ± 4.34% versus Let-blank: 18.65% ± 6.99%, $p = 0.046$] as early as 1 week after MI. Subsequently, more substantial differences in the LVEF [Let-miR-19b-1(+): 53.91% ± 6.69%

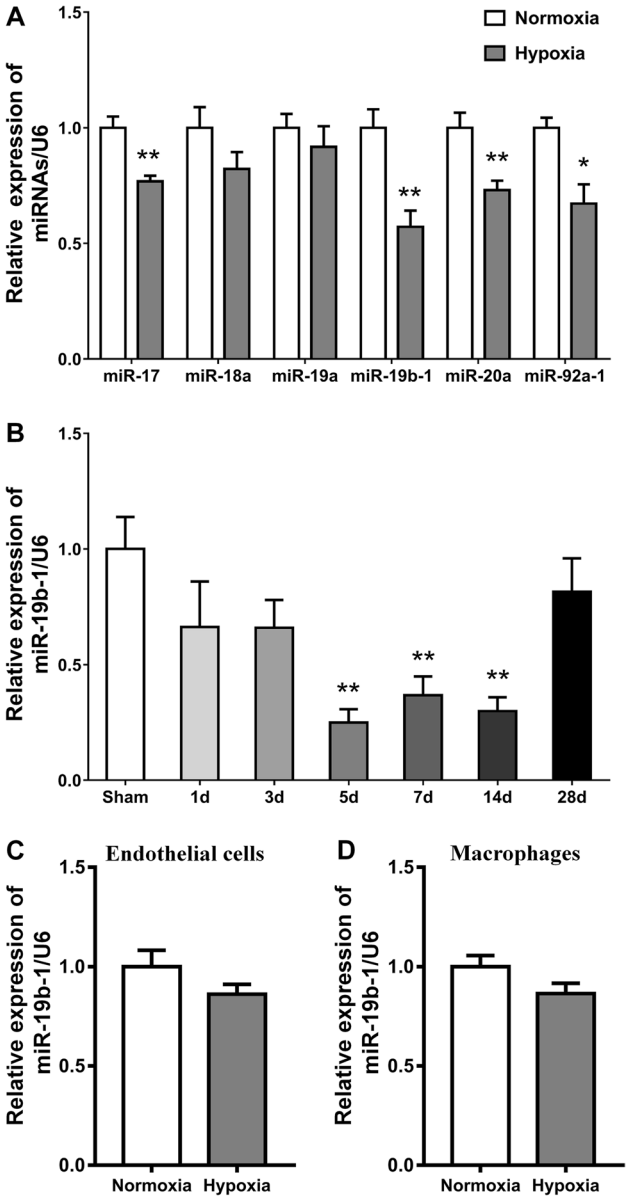

Fig. 1 Ischaemia suppressed cardiac miR-19b-1 expression in vitro and in vivo. **a** The expression of miR-19b-1 and its related miRNAs in the miR-17/92 cluster was downregulated in hypoxic cardiomyocytes. Among the miRNAs in the miR-17/92 cluster, the expression of miR-19b-1 was suppressed to the greatest extent in hypoxic cardiomyocytes. **b** The levels of miR-19b-1 in a mouse model of myocardial infarction were measured from days 1 to 28. The expression of miR-19b-1 exhibited a decreasing trend from days 1 to 14 but increased to a level similar to that in the sham group on day 28. $n = 5$ mice per group. However, no differences of miR-19b-1 expression levels were observed in endothelial cells (**c**, $p = 0.222$) and macrophages (**d**, $p = 0.150$) between hypoxia group and normoxia group. The cells were exposed to hypoxia or normoxia for 3 h before harvest. $^*p < 0.05$; $^{**}p < 0.01$

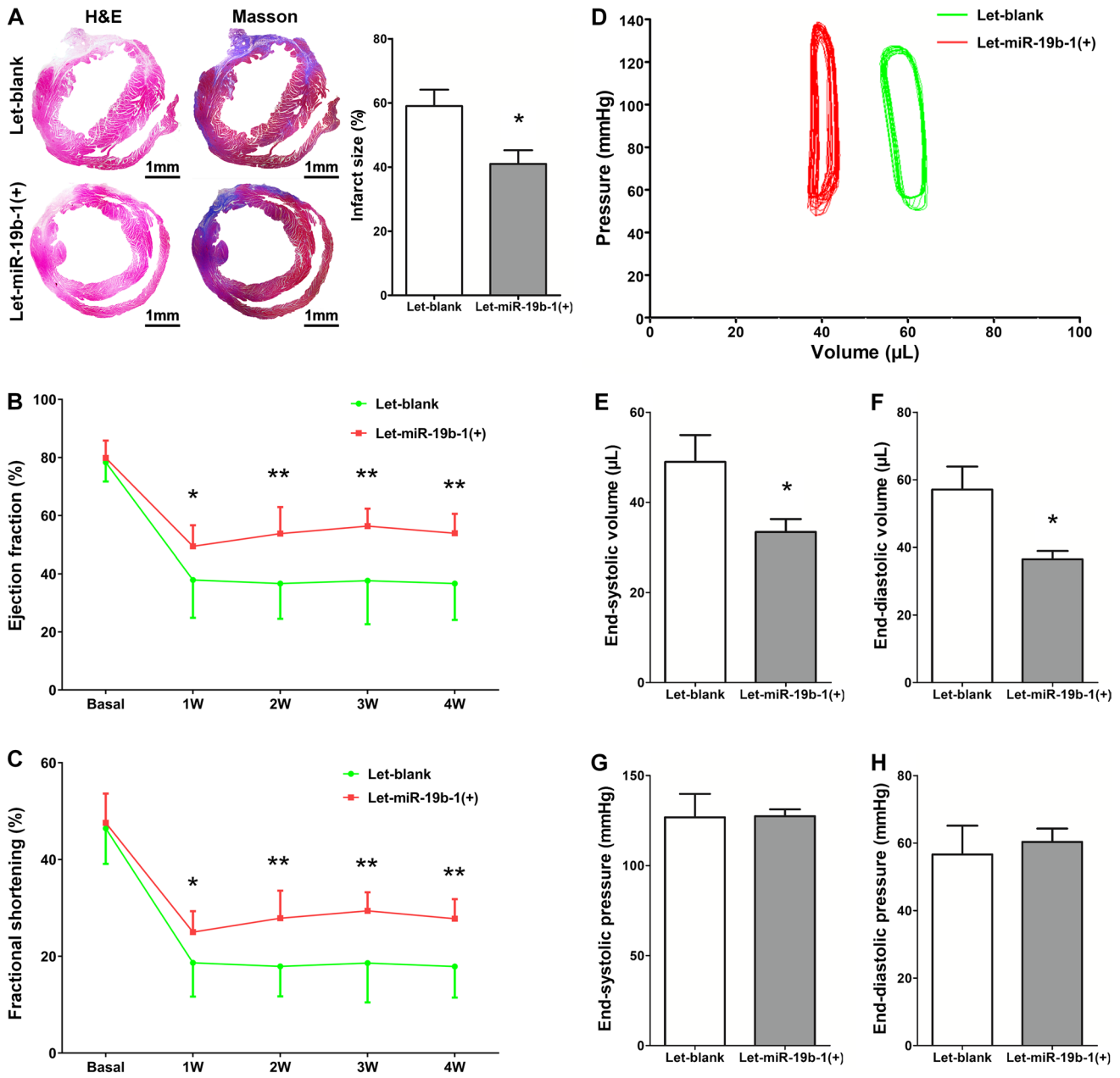

Fig. 2 MiR-19b-1 decreased the infarct area and restored the left ventricular cardiac function in mice with ischaemia-induced HF. **a** Images of haematoxylin and eosin (H&E) and Masson's trichrome staining performed at 4 weeks after myocardial infarction in the Let-miR-19b-1 and Let-blank groups. The infarct size was much smaller in the Let-miR-19b-1 group than in the Let-blank group. $n=6$ mice per group. **b**, **c** MiR-19b-1 preserved the left ventricular ejection fraction and fractional shortening in myocardial infarction-induced heart failure. $n=8$ mice per group. **d** The pressure–volume loop shifted to the left in mice with myocardial infarction transfected with the miR-19b-1 lentivirus compared with the lentivirus vector group. $n=5$ mice per group. **e**, **f** In the Let-miR-19b-1(+) mice, the end-systolic and end-diastolic volumes were smaller than those in the Let-blank mice. **g**, **h** No differences in the end-systolic and end-diastolic pressures were observed between the Let-miR-19b-1(+) and Let-blank groups. *$p<0.05$; **$p<0.01$

versus Let-blank: 36.69% ± 12.56%, $p=0.004$] and FS [Let-miR-19b-1(+): 27.77% ± 4.05% versus Let-blank: 17.89% ± 6.42%, $p=0.002$] were observed at the 4th week (Fig. 2b, c).

Additionally, a pressure–volume system was applied to determine the effects of miR-19b-1 on the pressure and volume in mice with ischaemia-induced HF at the 4th week. In the Let-miR-19b-1(+) mice, the end-systolic volume [Let-miR-19b-1(+): 34.84 ± 6.39 μL versus Let-blank: 48.97 ± 13.34 μL, $p=0.046$] and end-diastolic volume [Let-miR-19b-1(+): 37.16 ± 5.41 μL versus Let-blank: 57.09 ± 15.20 μL, $p=0.021$] were less

than the values recorded in the Let-blank mice. However, no differences in the end-systolic pressure [Let-miR-19b-1(+): 130.20 ± 8.57 mmHg versus Let-blank: 126.79 ± 29.12 mmHg, $p = 0.964$] or end-diastolic pressure [Let-miR-19b-1(+): 63.11 ± 8.90 mmHg versus Let-blank: 56.60 ± 19.09 mmHg, $p = 0.703$] were observed between the Let-miR-19b-1(+) and Let-blank groups (Fig. 2d–h).

MiR-19b-1 alleviated ischaemia-induced cardiac apoptosis

The NC or miR-19b-1 mimic was transfected into cardiomyocytes, which were then exposed to hypoxic conditions as described above to determine whether miR-19b-1 improved the cardiac function in mice with post-MI HF by regulating ischaemia-induced cardiac apoptosis. TUNEL staining showed that hypoxia increased the percentage of apoptotic cardiomyocytes (NC = 11.37 ± 3.82%), but the percentage of apoptotic cells in the miR-19b-1 mimic-transfected group decreased to approximately 0.33-fold of that in the NC group ($p = 0.031$, Fig. 3a).

Tissues from mice injected with Let-blank and Let-miR-19b-1(+) in the border zone of the infarcted myocardium were also stained with TUNEL. Substantially, fewer apoptotic cardiac cells were observed in the Let-miR-19b-1(+) group than in the Let-blank group. The apoptotic indexes were 30.21% ± 16.50% in the Let-miR-19b-1(+) group and 58.43% ± 10.90% in the Let-blank group ($p = 0.013$, $n = 5$ mice per group; Fig. 3b). Even though miR-19b-1 was reported to inhibit angiogenesis [21, 22], this phenomenon was not observed in MI mice infected with miR-19b-1-overexpressing lentivirus. There was no difference of CD31 staining in the infarcted myocardium between Let-blank group and Let-miR-19b-1(+) group 4 weeks post the interventions (Fig. 3c). In addition, the difference of CD68 staining was also not observed between Let-blank group and Let-miR-19b-1(+) group 4 weeks post the interventions. (Fig. 3d).

MiR-19b-1 reduced the Bcl2 l11 expression in cardiomyocytes

Primary cardiomyocytes were isolated and transfected with the NC or miR-19b-1 mimic, and the relative expression of apoptosis-related genes was measured to identify the target genes of miR-19b-1. Only the Bcl2 l11 mRNA was effectively downregulated by the miR-19b-1 mimic ($p = 0.003$), which was also confirmed by the western blot assay ($p = 0.038$). Subsequently, binding sites for miR-19b-1 in the Bcl2 l11 3′-UTR were predicted using TargetScan (https://www.targetscan.org/mmu_71). After co-transfection with miR-19b-1 mimics and 3′-UTR-Bcl2 l11-wt, the luciferase activity was significantly decreased in 293T cells ($p = 0.009$), whereas this effect was completely eliminated by replacing the wild-type vector with its mutant version (3′-UTR-Bcl2 l11-mut), as shown in Fig. 4.

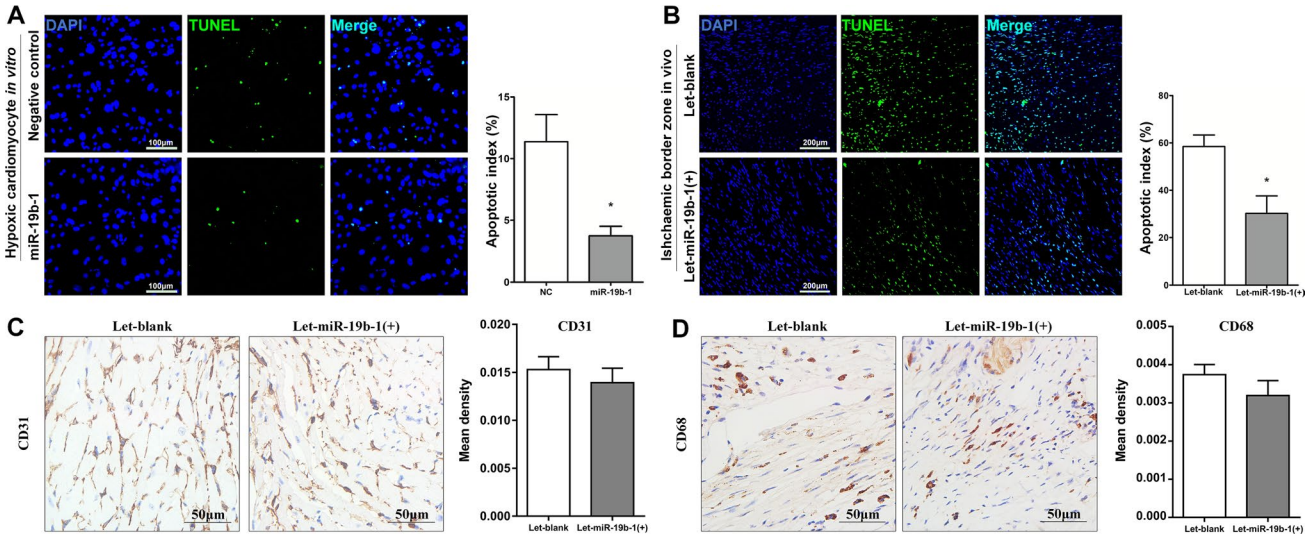

Fig. 3 MiR-19b-1 alleviated ischaemia-induced cardiac apoptosis in vivo and in vitro. **a** TUNEL staining was employed to detect the apoptosis of hypoxic cardiomyocytes transfected with the negative control or miR-19b-1 mimic. Unlike the negative control treatment, miR-19b-1 alleviated the hypoxia-induced cardiomyocyte apoptosis. **b** TUNEL staining of the infarct border zone revealed much less cardiac apoptosis in the Let-miR-19b-1(+) group than in the Let-blank group at the 1st week after myocardial infarction. In addition, no differences of CD31 (**c**) and CD68 (**d**) expression levels were observed in the infarcted myocardium 4 weeks post the interventions between Let-blank group and Let-miR-19b-1(+) group. $n = 5$ mice per group $^*p < 0.05$

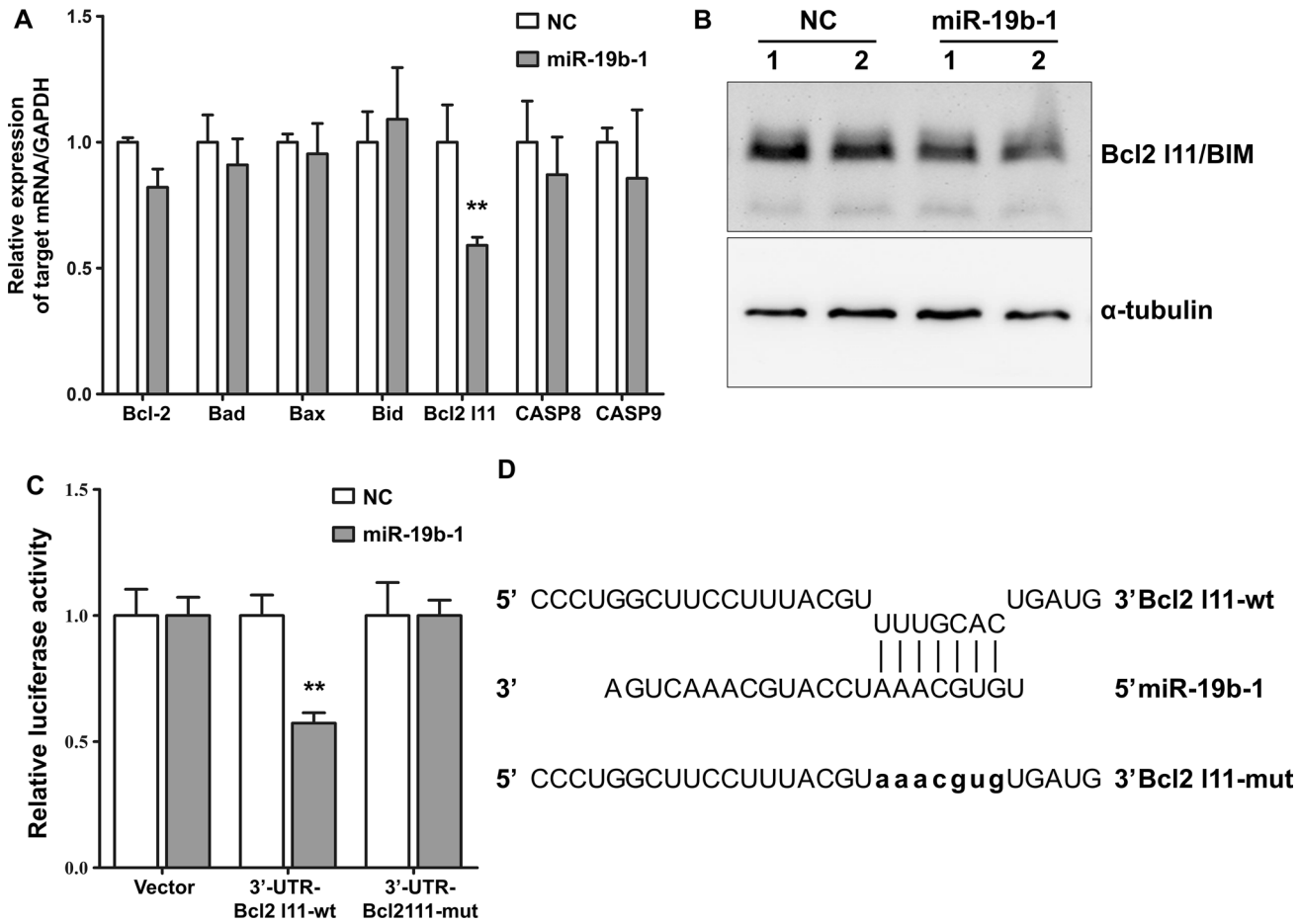

Fig. 4 MiR-19b-1 reduced Bcl2 l11 expression in cardiomyocytes. **a** The mRNA expression of Bcl2 l11 in cardiomyocytes was effectively downregulated by the miR-19b-1 mimic. **b** The western blot assay confirmed the effect of miR-19b-1 on reducing Bcl2 l11/BIM expression in cardiomyocytes. **c** The luciferase activity of 3′-UTR-Bcl2 l11-wt was significantly decreased by co-transfection of the miR-19b-1 mimic, whereas this effect was completely eliminated by replacing this vector with its mutant version (3′-UTR-Bcl2 l11-mut). $^{**}p < 0.01$

Discussion

In this study, MI-induced cardiac cell apoptosis and reduced miR-19b-1 expression was observed both in vivo and in vitro. However, miR-19b-1 overexpression decreased the infarct area and restored the left ventricular systolic function and volume load of mice with post-MI HF by inhibiting cardiac apoptosis. Moreover, miR-19b-1 targeted and downregulated the expression of Bcl2 l11/BIM, a classic proapoptotic member of the Bcl-2 family.

In previous studies, the miR-17/92 cluster was a critical regulator of cardiomyocyte proliferation in postnatal and adult hearts [23]. The expression of the miR-17/92 cluster was reduced in ischaemia–reperfusion mice [24]. Consistent with these results, hypoxia downregulated the expression of the miR-17/92 cluster in cardiomyocytes in the present study. Furthermore, miR-19b-1 exhibited the most significant decrease in expression among the miR-17/92 cluster, which suggested the crucial role of miR-19b-1 in myocardial ischaemia. However, HF after MI is a long-term pathological process that progresses from an acute to chronic phase [25], and the expression of miR-19b-1 exhibits a 'U-style' curve during the post-MI HF pathological process. In particular, miR-19b-1 expression exhibited a rapid tendency to decrease in the first week after surgery and was maintained at a low concentration for 2 weeks, but the trend then reversed, and the concentration reached a level approximately equal to that in the sham group at the 4th week. Thus, miR-19b-1 participates in acute ischaemia-induced myocardial injury and chronic heart remodelling. Our research revealed a protective function for miR-19b-1 in relieving post-MI HF. Overexpression of miR-19b-1 resulted in a decrease in the infarct area, an increase in the left ventricular systolic function, a decrease in the cardiac volume load, and a decrease in cardiomyocyte apoptosis. Moreover, miR-19b-1 was confirmed to directly target the proapoptotic gene Bcl2 l11/

BIM and inhibition of BIM has been reported to result in less apoptosis of MI hearts in mice [26]. According to a previous study, miR-19b-1 activates the PI3K/Akt pathway to increase cardiomyocyte survival by targeting phosphatase and tensin homologue (PTEN) [27–29]; in addition, activation of PI3K/AKT inhibits the expression of Bcl2 l11/BIM [30, 31]. Thus, miR-19b-1 targets multiple apoptosis-related genes to regulate cardiac apoptosis.

Although the MI-induced opening of collateral circulation partially improved the cardiac blood supply, it was not sufficient to reverse the large-scale myocardial apoptosis, which caused typical signs of HF, such as ventricular wall thinning, reduction in the LVEF and increase in the cardiac volume load. However, current clinical treatments lack the ability to antagonise cardiomyocyte apoptosis, which is an insurmountable difficulty limiting the effectiveness of the current therapies for post-MI HF. In this study, miR-19b-1 overexpression exerted a significant anti-apoptotic effect and improved the cardiac function in mice with MI-induced HF. However, the restoration of the miR-19b-1 level at the 4th week did not improve cardiac function in mice with post-MI HF. Several possible reasons may explain these contradictory findings. First, miR-19b-1 overexpression exerted an enhanced anti-apoptotic effect on cardiomyocytes, which helped the cells to survive the most dangerous period occurring early after ischaemia. Second, in the natural pathophysiological process of post-MI HF, the recovery of miR-19b-1 levels occurred late after ischaemia when apoptotic cardiomyocytes permanently lost their viability. Third, miR-19b-1 overexpression decreased the volume load in ischaemic hearts, which allowed more blood flow to restore dying cardiomyocytes. Thus, interventions performed at an early stage of ischaemia are the best therapeutic approach to prevent ischaemic hearts from progressing to HF, and increasing miR-19b-1 levels represent the best gene intervention to meet this requirement.

In summary, our study suggests that miR-19b-1 inhibits cardiac apoptosis and ameliorates cardiac function in mice with ischaemia-induced HF by targeting Bcl2 l11/BIM. These findings lay the theoretical foundation for the application of miR-19b-1 as a potential therapy for post-MI HF in the future.

Acknowledgements This work was supported by the National Natural Science Foundation of China (81670266 and 81770384), the Science and Technology Commission of Shanghai Municipality (17140902500) and Joint Funds for the innovation of science and Technology, Fujian province (2017Y9007).

Compliance with ethical standards

Conflict of interest The authors declare that they have no conflict of interest.

References

1. Yancy CW, Jessup M, Bozkurt B, Butler J, Casey DJ, Colvin MM, Drazner MH, Filippatos GS, Fonarow GC, Givertz MM, Hollenberg SM, Lindenfeld J, Masoudi FA, McBride PE, Peterson PN, Stevenson LW, Westlake C (2017) 2017 ACC/AHA/HFSA focused update of the 2013 ACCF/AHA guideline for the management of heart failure: a report of the American College of Cardiology/American Heart Association Task Force on clinical practice guidelines and the Heart Failure Society of America. J Am Coll Cardiol 70:776–803
2. Toischer K, Zhu W, Hunlich M, Mohamed BA, Khadjeh S, Reuter SP, Schafer K, Ramanujam D, Engelhardt S, Field LJ, Hasenfuss G (2017) Cardiomyocyte proliferation prevents failure in pressure overload but not volume overload. J Clin Investig 127:4285–4296
3. Bergmann O, Bhardwaj RD, Bernard S, Zdunek S, Barnabé-Heider F, Walsh S, Zupicich J, Alkass K, Buchholz BA, Druid H, Jovinge S, Frisén J (2009) Evidence for cardiomyocyte renewal in humans. Science 324:98–102
4. Dong Y, Liu C, Zhao Y, Ponnusamy M, Li P, Wang K (2018) Role of noncoding RNAs in regulation of cardiac cell death and cardiovascular diseases. Cell Mol Life Sci 75:291–300
5. Mogilyansky E, Rigoutsos I (2013) The miR-17/92 cluster: a comprehensive update on its genomics, genetics, functions and increasingly important and numerous roles in health and disease. Cell Death Differ 20:1603–1614
6. Sengupta D, Govindaraj V, Kar S (2018) Alteration in microRNA-17-92 dynamics accounts for differential nature of cellular proliferation. FEBS Lett 592:446–458
7. Ventura A, Young AG, Winslow MM, Lintault L, Meissner A, Erkeland SJ, Newman J, Bronson RT, Crowley D, Stone JR, Jaenisch R, Sharp PA, Jacks T (2008) Targeted deletion reveals essential and overlapping functions of the miR-17 through 92 family of miRNA clusters. Cell 132:875–886
8. Li S, Ren J, Xu N, Zhang J, Geng Q, Cao C, Lee C, Song J, Li J, Chen H (2014) MicroRNA-19b functions as potential antithrombotic protector in patients with unstable angina by targeting tissue factor. J Mol Cell Cardiol 75:49–57
9. Beaumont J, Lopez B, Ravassa S, Hermida N, Jose GS, Gallego I, Valencia F, Gomez-Doblas JJ, de Teresa E, Diez J, Gonzalez A (2017) MicroRNA-19b is a potential biomarker of increased myocardial collagen cross-linking in patients with aortic stenosis and heart failure. Sci Rep 7:40696
10. Hackl M, Brunner S, Fortschegger K, Schreiner C, Micutkova L, Muck C, Laschober GT, Lepperdinger G, Sampson N, Berger P, Herndler-Brandstetter D, Wieser M, Kuhnel H, Strasser A, Rinnerthaler M, Breitenbach M, Mildner M, Eckhart L, Tschachler E, Trost A, Bauer JW, Papak C, Trajanoski Z, Scheideler M, Grillari-Voglauer R, Grubeck-Loebenstein B, Jansen-Durr P, Grillari J (2010) miR-17, miR-19b, miR-20a, and miR-106a are down-regulated in human aging. Aging Cell 9:291–296
11. Zhong C, Wang K, Liu Y, Lv D, Zheng B, Zhou Q, Sun Q, Chen P, Ding S, Xu Y, Huang H (2016) miR-19b controls cardiac fibroblast proliferation and migration. J Cell Mol Med 20:1191–1197
12. Tang Y, Zhang YC, Chen Y, Xiang Y, Shen CX, Li YG (2015) The role of miR-19b in the inhibition of endothelial cell apoptosis and its relationship with coronary artery disease. Sci Rep 5:15132
13. Schober A, Weber C (2016) Mechanisms of microRNAs in atherosclerosis. Annu Rev Pathol 11:583–616
14. Mishra PK, Tyagi N, Kumar M, Tyagi SC (2009) MicroRNAs as a therapeutic target for cardiovascular diseases. J Cell Mol Med 13:778–789
15. Yang K, He YS, Wang XQ, Lu L, Chen QJ, Liu J, Sun Z, Shen WF (2011) MiR-146a inhibits oxidized low-density

lipoprotein-induced lipid accumulation and inflammatory response via targeting toll-like receptor 4. FEBS Lett 585:854–860
16. Mavrakis KJ, Van Der Meulen J, Wolfe AL, Liu X, Mets E, Taghon T, Khan AA, Setty M, Rondou P, Vandenberghe P, Delabesse E, Benoit Y, Socci NB, Leslie CS, Van Vlierberghe P, Speleman F, Wendel HG (2011) A cooperative microRNA-tumor suppressor gene network in acute T-cell lymphoblastic leukemia (T-ALL). Nat Genet 43:673–678
17. Baumgartner U, Berger F, Hashemi GA, Burgener SS, Monastyrskaya K, Vassella E (2018) miR-19b enhances proliferation and apoptosis resistance via the EGFR signaling pathway by targeting PP2A and BIM in non-small cell lung cancer. Mol Cancer 17:44
18. Puthalakath H, O'Reilly LA, Gunn P, Lee L, Kelly PN, Huntington ND, Hughes PD, Michalak EM, McKimm-Breschkin J, Motoyama N, Gotoh T, Akira S, Bouillet P, Strasser A (2007) ER stress triggers apoptosis by activating BH3-only protein Bim. Cell 129:1337–1349
19. Naftali-Shani N, Levin-Kotler LP, Palevski D, Amit U, Kain D, Landa N, Hochhauser E, Leor J (2017) Left ventricular dysfunction switches mesenchymal stromal cells toward an inflammatory phenotype and impairs their reparative properties via toll-like receptor-4. Circulation 135:2271–2287
20. Ramjee V, Li D, Manderfield LJ, Liu F, Engleka KA, Aghajanian H, Rodell CB, Lu W, Ho V, Wang T, Li L, Singh A, Cibi DM, Burdick JA, Singh MK, Jain R, Epstein JA (2017) Epicardial YAP/TAZ orchestrate an immunosuppressive response following myocardial infarction. J Clin Investig 127:899–911
21. Yin R, Guo L, Gu J, Li C, Zhang W (2018) Over expressing miR-19b-1 suppress breast cancer growth by inhibiting tumor microenvironment induced angiogenesis. Int J Biochem Cell Biol 97:43–51
22. Yin R, Bao W, Xing Y, Xi T, Gou S (2012) MiR-19b-1 inhibits angiogenesis by blocking cell cycle progression of endothelial cells. Biochem Biophys Res Commun 417:771–776
23. Chen J, Huang ZP, Seok HY, Ding J, Kataoka M, Zhang Z, Hu X, Wang G, Lin Z, Wang S, Pu WT, Liao R, Wang DZ (2013) mir-17-92 cluster is required for and sufficient to induce cardiomyocyte proliferation in postnatal and adult hearts. Circ Res 112:1557–1566
24. Xu J, Tang Y, Bei Y, Ding S, Che L, Yao J, Wang H, Lv D, Xiao J (2016) miR-19b attenuates H2O2-induced apoptosis in rat H9C2 cardiomyocytes via targeting PTEN. Oncotarget 7:10870–10878
25. Gyöngyösi M, Winkler J, Ramos I, Do Q, Firat H, McDonald K, González A, Thum T, Díez J, Jaisser F, Pizard A, Zannad F (2017) Myocardial fibrosis: biomedical research from bench to bedside. Eur J Heart Fail 19:177–191
26. Qian L, Van Laake LW, Huang Y, Liu S, Wendland MF, Srivastava D (2011) miR-24 inhibits apoptosis and represses Bim in mouse cardiomyocytes. J Exp Med 208:549–560
27. Jiang S, Li C, Olive V, Lykken E, Feng F, Sevilla J, Wan Y, He L, Li QJ (2011) Molecular dissection of the miR-17-92 cluster's critical dual roles in promoting Th1 responses and preventing inducible Treg differentiation. Blood 118:5487–5497
28. Chen CL, Tseng YW, Wu JC, Chen GY, Lin KC, Hwang SM, Hu YC (2015) Suppression of hepatocellular carcinoma by baculovirus-mediated expression of long non-coding RNA PTENP1 and MicroRNA regulation. Biomaterials 44:71–81
29. Liu SQ, Jiang S, Li C, Zhang B, Li QJ (2014) miR-17-92 cluster targets phosphatase and tensin homology and Ikaros Family Zinc Finger 4 to promote TH17-mediated inflammation. J Biol Chem 289:12446–12456
30. Rao E, Jiang C, Ji M, Huang X, Iqbal J, Lenz G, Wright G, Staudt LM, Zhao Y, McKeithan TW, Chan WC, Fu K (2012) The miRNA-17 approximately 92 cluster mediates chemoresistance and enhances tumor growth in mantle cell lymphoma via PI3K/AKT pathway activation. Leukemia 26:1064–1072
31. Shukla S, Bhaskaran N, Babcook MA, Fu P, Maclennan GT, Gupta S (2014) Apigenin inhibits prostate cancer progression in TRAMP mice via targeting PI3K/Akt/FoxO pathway. Carcinogenesis 35:452–460